Journal of Sound and Vibration (2000) **230**(4), 825–849
doi:10.1006/jsvi.1999.2657, available online at http://www.idealibrary.com on IDEAL®

A METHOD FOR THE VIBRATION ANALYSIS OF BUILT-UP STRUCTURES, PART I: INTRODUCTION AND ANALYTICAL ANALYSIS OF THE PLATE-STIFFENED BEAM

R. M. GRICE AND R. J. PINNINGTON

Institute of Sound and Vibration Research, University of Southampton, Southampton, SO17 1BJ, England

(*Received* 13 *April* 1999, *and in final form* 16 *September* 1999)

This is the first of two companion papers which collectively present a method for the analysis of built-up structures. One such structure is the machinery foundation of a ship which is constructed from a collection of large beams and flexible plates. The heavy vibration sources are supported by the large stiff beams. The power injected into and the power transmitted around the structure is controlled by long-wavelength waves generated in these beams by the vibration sources. As these long waves propagate along the stiff beams they generate short-wavelength flexural waves in the attached flexible plates. The long waves transmit some of their energy to the short-wavelength waves which therefore damp the long waves. The difference between the wavelengths of the long waves in the stiff beams and the short waves in the flexible plates is often very large. In this case, the short waves present a locally reacting impedance to the long waves at the structural joints. This paper argues that such a condition allows the vibration to predicted in three steps. First, the long-wave response of the stiff beams is analyzed in isolation of the short-wave response of the flexible plates; second, the short-wave response of the flexible plates is analyzed in isolation of the long-wave response; third, the two separate responses are combined to yield the response of the complete structure due to both the long and the short waves. The method is applied to a simple plate-stiffened beam consisting of a directly excited stiff beam attached to a large flexible plate which is broadly representative of the machinery foundation. The method predicts the frequency response of the plate-stiffened beam which compares well with laboratory measurements, thereby supporting the method. In this paper, all three steps are performed analytically which restricts the method to geometrically simple structures. The companion paper presents a hybrid numerical/analytical implementation which accommodates geometrically more diverse structures.

1. INTRODUCTION

This paper and its companion [1] are concerned with the vibration analysis of structures built up from beams and plates, an example of which is the machinery foundation of a ship.

0022-460X/00/090825 + 25 $35.00/0

Figure 1 shows a sketch of a ship machinery foundation which illustrates its main features. It consists of a number of very stiff beams (the frames) onto which heavy machinery is mounted, and a number of very flexible plates (the top plate and outer hull) which do not carry significant machinery loads. Because the machinery is mounted on the stiff beams they control the power injected into the complete structure [2]. The speed of waves in the beams is high and so it is also reasonable to expect that they form the primary path for vibration transmission [3, 4]. Flexural waves travelling along the stiff beams radiate short-wavelength flexural waves into the flexible plates which remove energy from the beams. The plates can therefore be viewed generally as dampers, although they obviously also affect the mass and stiffness of the complete structure. In this manner, the vibrational field in the machinery foundation develops into a mixture of long- and short-wavelength waves [5]. Henceforth for brevity, the terms *long wave* and *short wave* will be used instead of *long-wavelength flexural wave* and *short-wavelength flexural wave* respectively.

The above example illustrates how the vibrational power injected from machinery mounted on the stiff parts of the built-up structure becomes split between long waves travelling in the stiff parts and short waves travelling in the flexible parts. The relative proportions of the total power carried by the two waves depends on the inherent damping of the long waves (e.g., the material loss factor of the stiff parts) and the level of coupling between the two waves at the joints where the stiff and flexible parts meet. This means that the damping of the long waves can be increased if more energy can be transmitted to the short waves, an observation which provides one potential vibration control methodology for built-up structures.

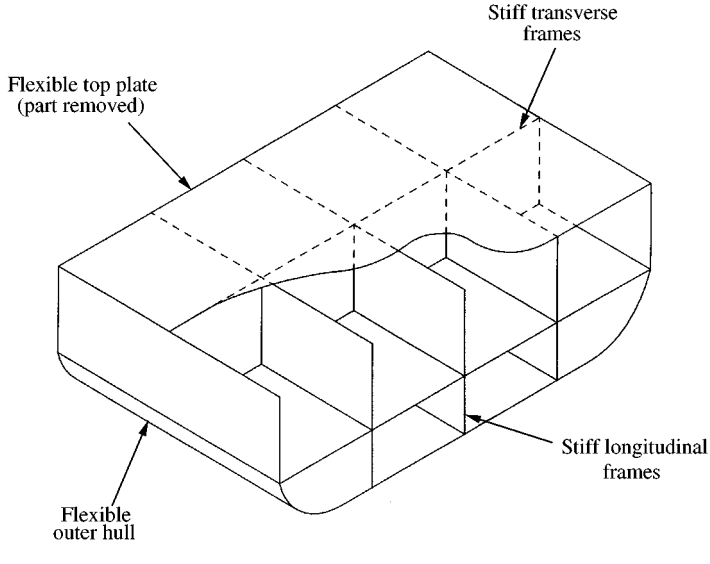

Figure 1. Sketch of a typical machinery foundation of a ship.

In the machinery foundation, the wavelengths of the long waves in the stiff beams may be much greater than that of the short waves in the flexible plates. The difference in wavelengths can be problematic for the methods presently available for the analysis of built-up structures such as finite element analysis and statistical energy analysis. For example, in finite element analysis the element size is generally determined by the shortest wavelength of all the wave types which exist in the structure at any particular frequency. In the built-up structure, the element size will be determined by the wavelength of the short waves in the flexible plates and so many elements will be required to obtain adequate numerical accuracy. Unfortunately, the resultant finite element mesh may be too large to analyze in an acceptable time. Alternatively, the long waves in the stiff beams may have so low a modal density that statistical energy analysis is inappropriate. Additionally, the vibration sources may act upon small areas of the structure (e.g., through vibration isolators) and/or have a predominantly tonal characteristic. These properties reduce modal density and undermine the condition of modal equipartition which is necessary to confidently apply statistical energy analysis [6].

A different approach to the analysis of built-up structures which has been adopted previously is to deliberately ignore the contribution of either the long or the short waves. For example, Gibbs and Gilford [7] used statistical energy analysis to analyze building structures using short flexural waves with or without long in-plane waves. The differences between the two predictions were not large but were subject to considerable uncertainty at low frequencies in the far field (i.e., when source and receiver are separated by many junctions) because the modal density of the long in-plane waves was small. Lyon [8] considered statistical energy analysis of a machinery foundation and also showed that neglecting the long in-plane waves caused considerable discrepancy in the farfield energy level predictions. These references suggest that in general the response of built-up structures excited on their stiff parts cannot be accurately predicted unless both the long and short waves are included. Thus, the overall objective of this paper and its companion is to introduce a method for the analysis of built-up structures which explicitly accommodates vibration formed from waves having significantly different wavelengths. The specific objectives of this paper will be detailed shortly.

1.1. PREVIOUS RESEARCH INTO STRUCTURES CHARACTERISTIC OF THE MACHINERY FOUNDATION

A number of researchers have investigated the behaviour of built-up structures characteristic of the machinery foundation by including both the long and the short waves as follows. Lamb [9] and Heckl [10] derived analytical expressions for the input mobility of the plate-stiffened beam shown in Figure 2. This structure consists of a single infinite beam driven directly by a force (i.e., on the stiff part) which is attached to an infinite plate. The directly driven beam was assumed to carry flexural waves whose wavelengths were much longer than those of the flexural waves in the plate. As a result the plate was idealized as a set of narrow strips of plate, effectively one-dimensionalizing the plate into a set of dynamic stiffness

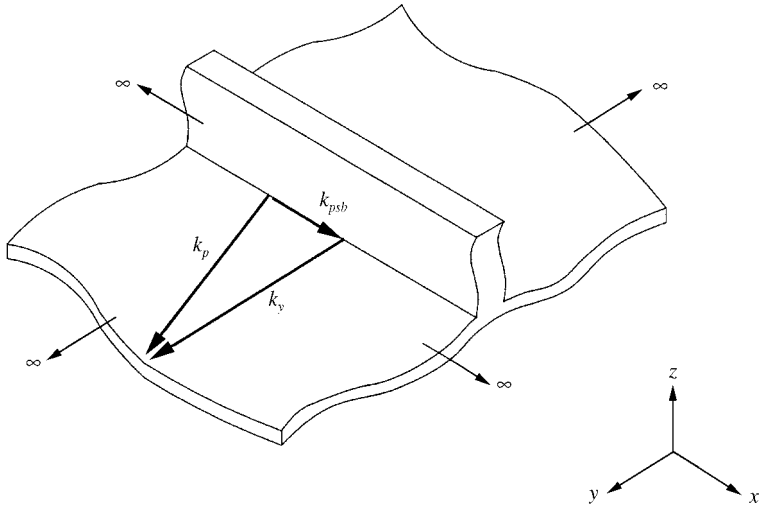

Figure 2. An infinite plate-stiffened beam consisting of a single infinite beam attached to an infinite plate. The wavenumber vector triangle shows the travelling waves only.

elements which only permit plate motion normal to the axis of the beam. This idealization means that the plate is modelled using a locally reacting impedance [11]. The mobility of the plate-stiffened beam yielded by Heckl's analysis was similar to that of the stiff beam on its own, thereby indicating that the beam controls the power input, but featured an additional term which showed that the idealized locally reacting plate acted as a frequency-dependent damper. Neither Lamb nor Heckl explicitly determined the frequency limitation of the locally reacting assumption which is crucial to correct application of their analyses. This paper will address this deficiency.

The present author [12, 13] measured the input and transfer mobilities of the finite plate-stiffened beam of Figure 3. While the characteristic response was beam-like, the measurements showed that transmission of the long flexural waves along the beam was strongly attenuated in narrow-frequency bands by the short flexural waves in the plate. Outside these narrow-frequency bands of high attenuation, transmission along the beam was largely unaffected by the plate. The existence of the narrow bands of high attenuation should provide a means of vibration control if the narrow bands can be predicted. Thus, this paper will present analysis which predicts the narrow bands of high attenuation.

1.2. THEORETICAL METHOD, OBJECTIVES AND LAYOUT OF THIS PAPER

The previous sections indicate that the response of built-up structures excited on their stiff parts is a combination of long waves and short waves which have the following contrasting characteristics.

(i) The long waves travelling in the stiff parts control both the power input and overall the power transmission through the structure. Henceforth, the stiff

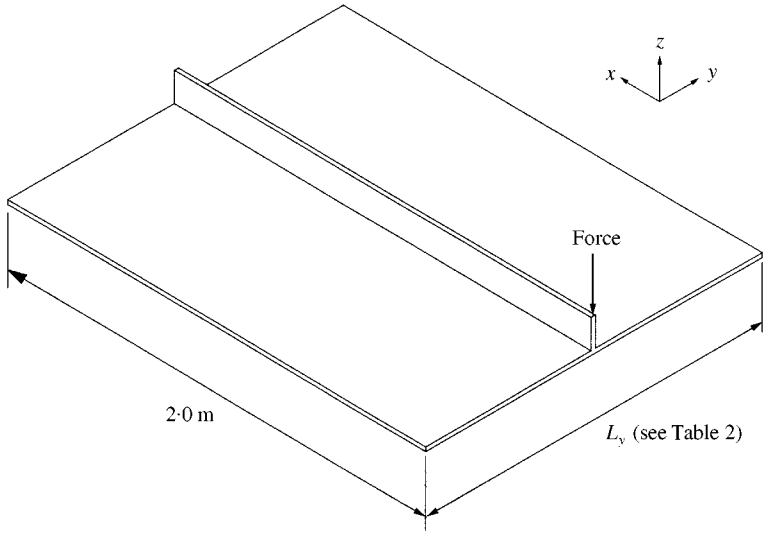

Figure 3. The experimental plate-stiffened beam. The force acts at one end of the beam as shown. The beam is 68 mm high excluding the thickness of the plate. Both beam and plate are 5·9 mm thick. The material properties are given in Table 1.

part will be referred to as the *spine* to indicate that it provides the primary vibration transmission path in the structure.

(ii) The long waves travelling in the spine generate short waves in the flexible parts at the interconnecting junctions. Henceforth, these flexible parts will be referred to as *receivers* to indicate that they receive vibrational energy from the spine rather than directly from the excitation.

(iii) On account of the large difference in the wavelengths of the waves travelling in the spine and the receivers, the receivers present a locally reacting impedance to the spine.

The theoretical method presented here is that the contrasting characteristics of the long and short waves permit the responses of the spine and of the receivers to be calculated separately, i.e., the complete structure is partitioned into two components, one of which represents the spine and the other represents the receivers. The responses of the spine and of the receivers are calculated separately and are subsequently combined to produce the response of the complete structure due to both wave types. Thus, the overall objectives of this paper and its companion are collectively as follows:

(a) to determine the relationship between the spine and receiver wavenumbers which permits application of the theoretical method;
(b) to determine the parameters needed to model the response of the receivers;
(c) to determine the parameters needed to model the response of the spine;
(d) to determine the parameters needed to model the response of the complete structure when the separate responses of the receivers and spine are combined.

There is a substantial amount of ground to be covered in explaining the method. Hence, this paper uses analysis of the plate-stiffened beam to specifically address only objectives (a) and (b). In passing, it will also be shown how to predict the narrow bands of high attenuation observed in reference [12]. Predictions of input and transfer frequency response for two different plate-stiffened beams are compared with laboratory measurements.

The material in this paper is insightful on its own but the analytical method is restricted to geometrically simple built-up structures. Therefore, the companion paper presents a numerical/analytical implementation which broadens the scope of the method to more complicated built-up structures. In doing so the companion paper addresses overall objectives (c) and (d).

2. WAVE ANALYSIS OF A PLATE-STIFFENED BEAM

The objective of this section is to determine analytical expressions for the input and transfer frequency response functions of the finite plate-stiffened beam shown in Figure 3. It is convenient to commence with analysis of the *infinite* plate-stiffened beam of Figure 2.

2.1. GENERAL DISPERSION RELATION FOR AN INFINITE BEAM COUPLED TO AN INFINITE PLATE

Figure 2 shows the structure under consideration. It consists of an infinite beam coupled along its lower edge to an infinite plate.

Initially when *uncoupled* from the plate, the beam carries a travelling wave of frequency ω and wavenumber k_b and so its displacement is

$$\tilde{u}_b = \tilde{A} e^{-j k_b x} e^{j\omega t}, \tag{1}$$

where $\tilde{A}$ is the amplitude (Appendix B contains a list of symbols). Henceforth the time dependence $e^{j\omega t}$ will be suppressed. When the beam and plate are joined together, the motion of the infinite plate (which is assumed to be symmetric on either side of the beam) is

$$\begin{aligned} \tilde{u}_{p^+} &= (\tilde{B} e^{-j k_y y} + \tilde{C} e^{-k_e y}) e^{-j k_{psb} x}, \quad y \geqslant 0, \\ \tilde{u}_{p^-} &= (\tilde{B} e^{+j k_y y} + \tilde{C} e^{+k_e y}) e^{-j k_{psb} x}, \quad y \leqslant 0, \end{aligned} \tag{2}$$

where $\tilde{B}$, $\tilde{C}$ are amplitudes, k_y is the wavenumber for the travelling wave radiating into the plate normal to the beam as in Figure 2, k_e is the wavenumber for the nearfield wave in the plate and k_{psb} is the *coupled* wavenumber in the beam. The beam drives the plate with a force per unit length $\tilde{f}'$ and has the following equation of motion:

$$\tilde{D}_b \frac{\partial^4 \tilde{u}_b}{\partial x^4} - m'_b \omega^2 \tilde{u}_b = -\tilde{f}' \tag{3}$$

where $\tilde{D}_b$, m'_b are the beam complex stiffness and mass per unit length respectively. The equation of motion for the plate is

$$D_p \nabla^4 \tilde{u}_p - m''_p \omega^2 \tilde{u}_p = 0, \quad \nabla^4 = \frac{\partial^4}{\partial x^4} + 2\frac{\partial^4}{\partial x^2 \partial y^2} + \frac{\partial^4}{\partial y^4} \tag{4a,b}$$

where the free plate wavenumber k_p shown in Figure 2 is

$$k_p = \sqrt{\omega}\left(\frac{m_p''}{D_p}\right)^{1/4}, \quad m_p'' = \rho t, \quad D_p = \frac{Et^3}{12(1-\nu^2)}. \tag{5a–c}$$

The boundary conditions at the beam/plate joint are:

(i) The displacement of beam and plate are equal along the joint,

$$\tilde{u}_b(x) = \tilde{u}_p(x, 0). \tag{6}$$

(ii) The slope normal to the beam along the joint is zero,

$$\left.\frac{\partial \tilde{u}_p}{\partial y}\right|_{y=0} = 0 \tag{7}$$

(iii) If the plate is cut in two at the joint, the shear force applied to each half plate is [14]

$$D_p \frac{\partial}{\partial y}\left(\frac{\partial^2 \tilde{u}_{p^+}}{\partial y^2} + (2-\nu)\frac{\partial^2 \tilde{u}_{p^+}}{\partial x^2}\right)\bigg|_{y=0} = \frac{\tilde{f}'}{2}. \tag{8}$$

Equations (6) and (7) yield the amplitude of the waves in the plate (after a little algebra)

$$\tilde{B} = \frac{k_e^2 + \mathrm{j}k_e k_y}{k_e^2 + k_y^2}\tilde{A}, \quad \tilde{C} = \frac{k_y^2 - \mathrm{j}k_e k_y}{k_e^2 + k_y^2}\tilde{A}. \tag{9a,b}$$

Upon substituting equations (2) and (9) into the equation of motion of the plate, the wavenumbers in the plate are found to be

$$k_y = \sqrt{k_p^2 - k_{psb}^2}, \quad k_e = \sqrt{k_p^2 + k_{psb}^2}. \tag{10a,b}$$

The first expression in equation (10) represents trace-matching of the travelling waves at the joint as shown by the wavenumber vector triangle in Figure 2. Equation (8) then gives

$$\tilde{A}\mathrm{e}^{-\mathrm{j}k_{psb}x}(k_e k_y)(-k_y + \mathrm{j}k_e) = \frac{\tilde{f}'}{2D_p} \tag{11}$$

from which the dispersion relation for the infinite beam attached to the infinite plate is found using equation (3) to be

$$\tilde{D}_b k_{psb}^4 = m_b'\omega^2 + 2D_p(k_e k_y)(k_y - \mathrm{j}k_e). \tag{12}$$

This is a *general* dispersion relation for the beam coupled to the plate. It does not require the plate to be locally reacting. It will be used later once the condition under which the plate can be considered locally reacting has been established.

2.2. LINE IMPEDANCE OF AN INFINITE PLATE COUPLED TO AN INFINITE BEAM

The line impedance of the plate at its attachment to the beam (i.e., the impedance of the plate per unit length of the beam) is found by rearranging equation (11) to yield

$$\tilde{Z}_p' = \frac{2D_P}{\omega}(k_e k_y)(k_e + \mathrm{j}k_y). \tag{13}$$

This line impedance can be written in two forms. The exact impedance is found directly from equations (10) and (13) to be

$$\tilde{Z}'_p = \frac{2m''_p\omega}{k_p}\sqrt{1-(k_{psb}/k_p)^4}\,\{\sqrt{1+(k_{psb}/k_p)^2}+\mathrm{j}\sqrt{1-(k_{psb}/k_p)^2}\}. \tag{14}$$

For $k_p \gg k_{psb}$, equation (14) simplifies to

$$\tilde{Z}'_p|_{k_p \gg k_{psb}} \approx \frac{2m''_p\omega}{k_p}(1+\mathrm{j}) \tag{15}$$

which is recognizable as the input *point* impedance of a beam of infinite length and unit width driven by a point force [15]. Figure 4 shows the ratio of the approximate point impedance of equation (15) to the exact line impedance of equation (14) as a function of the wavenumber ratio k_{psb}/k_p. Provided the plate wavenumber is at least twice the coupled beam wavenumber, i.e., $k_{psb}/k_p < 0{\cdot}5$, the two impedances are within 3% of one another such that the plate can be regarded as locally reacting and the simpler expression of equation (15) can be used. This result addresses the deficiency in references [9, 10].

Physically speaking, the locally reacting impedance means that waves radiate into the plate at an angle which is almost normal to the axis of the beam [11], implying that the beam carries waves which are much longer than those in the plate. In accord with the theoretical method stated in section 1.2, the beam is therefore the *spine*. The plate carries short waves and is therefore the *receiver*. For a locally reacting infinite plate attached to the spine beam, equation (15) defines the corresponding *infinite receiver impedance*.

To illustrate the usefulness of Figure 4, Figure 5 shows the wavenumber ratio k_{psb}/k_p over the range 10 Hz to 1 kHz for the plate-stiffened beam of Figure 3 but with the plate of infinite extent. In this figure, the stiffness of the beam has been

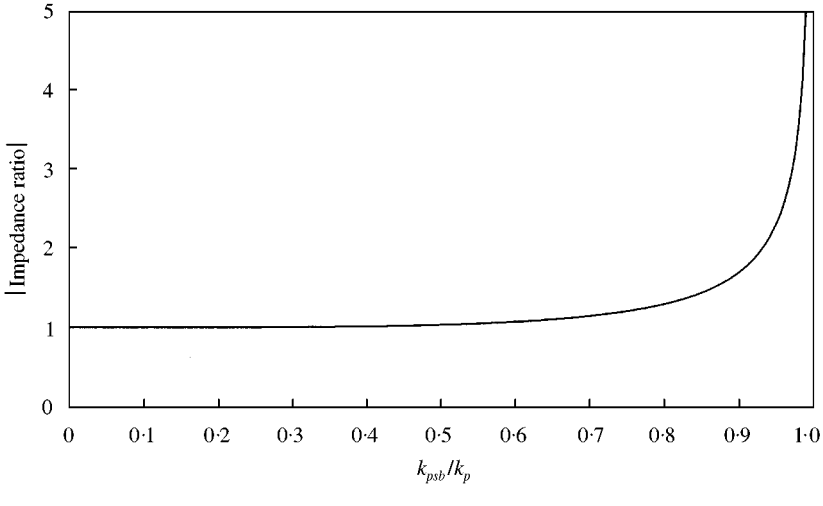

Figure 4. Ratio of the impedance of equation (15) to the impedance of equation (14) as a function of the ratio of the coupled beam wavenumber k_{psb} to the plate wavenumber k_p.

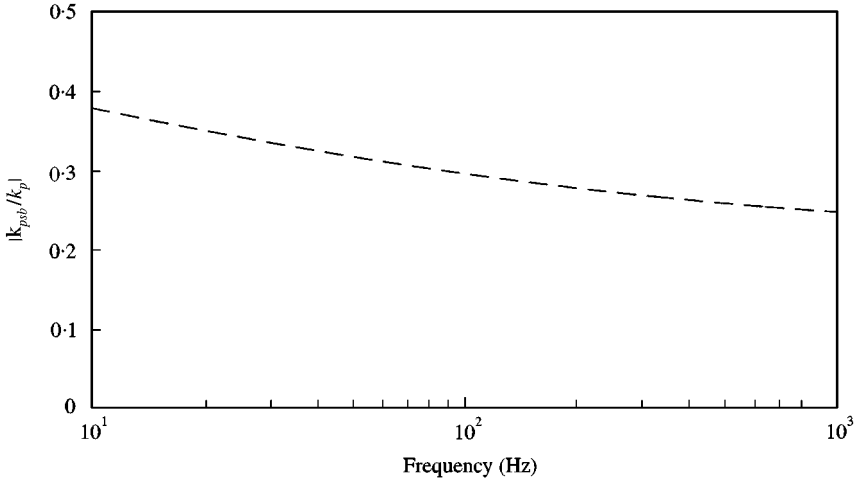

Figure 5. Ratio of the coupled wavenumber k_{psb} to the plate wavenumber k_p for the plate-stiffened beam of Figure 3 but with an infinite plate.

TABLE 1

Nominal material properties for the plate-stiffened beam

Young's modulus (GN/m^2)	Poisson's Ratio	Density (kg/m^3)
4·4	0·38	1152

calculated by assuming that the neutral axis lies in the mid-plane of the plate using

$$D_b = E\left[\frac{th^3}{12} + th\frac{(h+t)^2}{4}\right], \tag{16}$$

where the beam height h and thickness t are given in Figure 3 and the material properties are given in Table 1. Figure 5 shows that over the chosen frequency range the plate wavenumber is at least twice the beam wavenumber which means that the plate is locally reacting. Note that the wavenumber ratio is not frequency independent (as might be expected for two structures operating in flexure) because the coupled beam wavenumber is itself a function of the plate wavenumbers, as shown by equation (12).

2.3. GENERAL DISPERSION RELATION FOR AN INFINITE SPINE COUPLED TO A GENERAL LOCALLY REACTING RECEIVER IMPEDANCE

Having determined the condition under which the plate can be considered locally reacting, it is appropriate to consider the dispersion relation for a spine coupled to a *general* locally reacting receiver impedance.

The general dispersion relations derived at equation (12) can be rearranged to give (after some manipulation)

$$\tilde{D}_b k_{psb}^4 = m'_b \omega^2 - \mathrm{j}\omega \tilde{Z}^{R'} \tag{17}$$

where $\tilde{Z}^{R'}$ is *any* locally reacting impedance which may, of course, have an arbitrary frequency dependence. Equation (17) is recognizable as the dispersion relation for the spine beam together with an extra term featuring the receiver impedance. Although this analysis is couched in terms of dispersion in a beam, equation (17) is central to the present method because it states that the response of the complete structure can be found in three steps: first, the dispersion relation for the spine separate from the receiver is determined. Second, the locally reacting impedance of the receiver is established. Third, the spine dispersion relation and the receiver impedance are combined to obtain the response of the two parts coupled together. Hence, using the infinite receiver impedance of equation (15) in the general dispersion relation yields (after some manipulation)

$$\tilde{D}_b k_{psb}^4 = (m'_b + m'_{px})\omega^2(1 - \mathrm{j}\eta_{12}), \tag{18}$$

where $m'_{px} = m''_p \lambda_p / \pi$ is the mass per unit length along the beam of a piece of plate having a width of approximately one-third of the plate wavelength, and η_{12} is defined by

$$\eta_{12} = \frac{m'_{px}}{m'_b + m'_{px}}. \tag{19}$$

This last equation represents damping in the dispersion relation. It is in fact a coupling loss factor which accounts for the loss of energy from the spine to the receiver as waves travel down the spine. Typically, this coupling loss factor is large at low frequencies and decreases with frequency [10].

2.4. IMPEDANCE OF A FINITE WIDTH PLATE COUPLED TO AN INFINITE BEAM

The next step in developing the theory for the fully finite plate-stiffened beam of Figure 3 is to consider the structure shown in Figure 6 in which the plate has finite width L_y and is assumed for analytical and experimental simplicity to be symmetrical on either side of the infinite beam. This analysis is necessary because the narrow bands of high attenuation observed in references [12, 13] cannot be explained using the impedance of the infinite width plate.

In the symmetrical structure, the motion of the plate on either side of the beam is

$$\begin{aligned} \tilde{u}_{p^+} &= (\tilde{B}\mathrm{e}^{-\mathrm{j}\tilde{k}_y y} + \tilde{C}\mathrm{e}^{-k_e y} + \tilde{\beta}_y \tilde{r}\tilde{B}\mathrm{e}^{+\mathrm{j}\tilde{k}_y y} + \tilde{D}\mathrm{e}^{k_e(y - L_y/2)})\mathrm{e}^{-\mathrm{j}k_{psb}x}, \quad y \geqslant 0, \\ \tilde{u}_{p^-} &= (\tilde{B}\mathrm{e}^{+\mathrm{j}\tilde{k}_y y} + \tilde{C}\mathrm{e}^{+k_e y} + \tilde{\beta}_y \tilde{r}\tilde{B}\mathrm{e}^{-\mathrm{j}\tilde{k}_y y} + \tilde{D}\mathrm{e}^{-k_e(y - L_y/2)})\mathrm{e}^{-\mathrm{j}k_{psb}x}, \quad y \leqslant 0, \end{aligned} \tag{20}$$

where the wavenumber $\tilde{k}_y$ is now complex to accommodate material losses in the plate, k_e is as before, $\tilde{r}$ is the complex reflection coefficient at the edge of the plate and $\tilde{\beta}_y$ is

$$\tilde{\beta}_y = \mathrm{e}^{-\mathrm{j}\tilde{k}_y L_y}, \quad \beta_y = |\tilde{\beta}_y| = \mathrm{e}^{-(1/4)\eta_p k_y L_y} \tag{21}$$

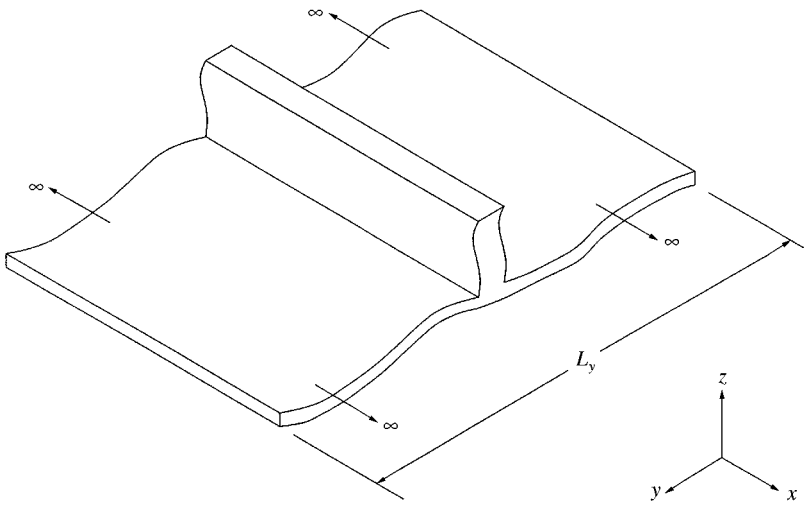

Figure 6. A plate-stiffened beam consisting of a single infinite beam attached to a finite width plate.

Using the equations of motion and the boundary conditions from section 2.1, the exact line impedance of the plate is found to be (after some manipulation)

$$\tilde{Z}'_p = \frac{2D_p}{\omega}(k_e k_y)(k_e + \mathrm{j}k_y)\frac{(k_e - \mathrm{j}k_y) - \tilde{\beta}_y \tilde{r}(k_e - \mathrm{j}k_y)}{(k_e - \mathrm{j}k_y) + \tilde{\beta}_y \tilde{r}(k_e + \mathrm{j}k_y)}. \tag{22}$$

For small values of the wavenumber ratio and using the travelling wave reflection coefficient for a free edge $\tilde{r} = -\mathrm{j}$ [15], equation (22) simplifies to

$$\tilde{Z}'_p\,|_{k_p \gg k_{psb}} \approx \frac{2m''_p\omega}{k_y}\left(\frac{1 - \tilde{\beta}_y}{1 + \tilde{\beta}_y} + \mathrm{j}\right). \tag{23}$$

Equation (23) is the *point* impedance per unit width of a finite length beam driven at its mid-point carrying a wavenumber $\tilde{k}_y$. Thus, provided the plate wavenumber is at least twice the beam wavenumber, the finite width plate still presents a locally reacting impedance to the beam. Equation (23) is the finite analogue of the infinite receiver impedance of equation (15) and is therefore called the *finite receiver impedance*. It is essentially a function of two parameters: first, the width L_y of the receiver normal to the spine since this determines $\tilde{\beta}_y$; second, the wavenumber $\tilde{k}_y$ which describes radiation of waves into the receiver normal to the spine. Accordingly, this wavenumber is defined as the *receiver wavenumber*.

Of course, the receiver wavenumber $\tilde{k}_y$ in equation (23) is not known precisely because it depends on the coupled beam which is implicit in the finite receiver impedance. In the present case, a closed-form solution for the receiver wavenumber could not be found so the dispersion relation was solved iteratively. A first estimate for $\tilde{k}_y$ was found by assuming the plate to have *infinite* width using equation (10a) in the form

$$\tilde{k}_y \approx \sqrt{k_p^2 - k_{psb}^2}\left(1 - \mathrm{j}\frac{\eta_p}{4}\right). \tag{24}$$

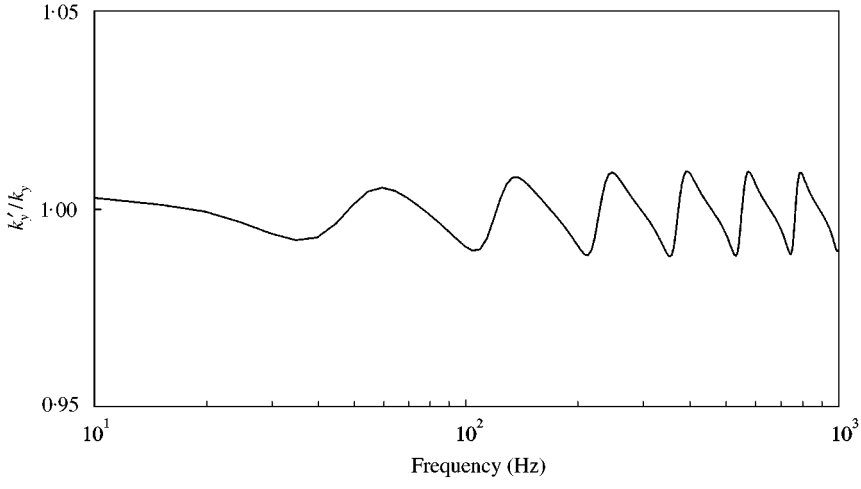

Figure 7. Ratio of the second estimate of the finite receiver wavenumber k_y' to the first estimate of k_y calculated using equation (24).

where k_{psb} is found from equation (17) with the *infinite* receiver impedance of equation (15), and η_p accommodates the inherent damping of the plate. Equation (24) was then applied to calculate an estimate for the finite receiver impedance with equation (23). This was used to determine a second estimate for the wavenumber $\tilde{k}_y$. For the structure of Figure 3 convergence occurred rapidly, and Figure 7 shows the ratio of the second estimate of k_y (denoted k_y') to the first estimate of k_y from equation (24). The graph shows that in the present case, equation (24) is a satisfactory estimate for the finite receive wavenumber.

2.5. WAVENUMBER FOR THE SPINE BEAM COUPLED TO A FINITE RECEIVER PLATE

Using the finite receiver impedance of equation (23), the general dispersion relation of equation (17) for the spine beam attached to the finite width receiver plate becomes

$$\tilde{D}_b k_{psb}^4 \approx (m_b' + m_{px}')\omega^2 \left\{1 - \mathrm{j}\eta_{12}\left(\frac{1-\tilde{\beta}_y}{1+\tilde{\beta}_y}\right)\right\}. \tag{25}$$

The coupling loss factor remains as defined previously in equation (19). The dispersion relation now features a dynamic magnification factor which in general is complex and so it is not possible to deduce a straightforward expression for the spine wavenumbers. However, observations can be made for two important values of the finite receiver impedance as follows.

2.5.1. *Receiver resonance*

The receiver *resonance* frequencies occur when the drive-point velocity is maximized. At these frequencies, the imaginary part of the finite receiver impedance

vanishes [15] and equation (23) becomes

$$\tilde{Z}'_p \approx \frac{2m''_p\omega}{k_y}\left(\frac{1-\beta_y^2}{1+\beta_y^2}\right). \tag{26}$$

The dispersion relation of equation (17) is then

$$\tilde{D}_b k_{psb}^4 \approx \omega^2 \left\{ m'_b - \mathrm{j}m'_{px}\left(\frac{1-\beta_y^2}{1+\beta_y^2}\right)\right\} \tag{27}$$

where the terms in β_y are small. Hence, when the spine is attached to a finite resonant receiver the transmission of flexural waves along the spine is not greatly affected by the receiver. Physically speaking, this result can be explained on the basis that at resonance the receiver is very mobile and so presents little dynamic load to the spine.

2.5.2. *Receiver antiresonance*

When the receiver driven by the force at its mid-point is anti-resonant (i.e., the drive-point velocity is minimized), the impedance becomes

$$\tilde{Z}'_p = \frac{2m''_p\omega}{k_y}\left(\frac{1+\beta_y}{1-\beta_y} + \mathrm{j}\right\}. \tag{28}$$

The first term in the parentheses is real and will be large if the receiver internal loss factor is small. This is the maximum value which the real part of the impedance can attain. The dispersion relation then becomes (after expanding the complex stiffness)

$$D_b k_{psb}^4 \approx (m'_b + m'_{px})\omega^2 \left\{\left[1 - \eta_b\eta_{12}\left(\frac{1+\beta_y}{1-\beta_y}\right)\right] - \mathrm{j}\left[\eta_b + \eta_{12}\left(\frac{1+\beta_y}{1-\beta_y}\right)\right]\right\}. \tag{29}$$

The dispersion relations shows that the real part diminishes and the imaginary part increases. It may now yield so-called "complex" waves [16, 17] which decay rapidly and thus reduce transmission along the spine. Physically speaking, at anti-resonance the finite receiver "blocks" the motion of the spine.

2.6. INPUT AND TRANSFER MOBILITIES OF A FINITE PLATE-STIFFENED BEAM

Thus far, expressions have been deduced for the dispersion relation which describes the propagation of waves along an infinite spine beam attached to a receiver plate of either infinite or finite width. The dispersion relation can now be used to derive the mobilities for the fully finite structure shown in Figure 3.

The input and transfer mobilities of a finite Euler–Bernoulli beam of length L_b with both ends free and driven by a force at one end are [18, 19]

$$\tilde{Y}_1 = \frac{k_b}{m'_b\omega}\left(\frac{1-\tilde{\alpha}_b}{1+\tilde{\alpha}_b} - \mathrm{j}\right), \quad \tilde{Y}_{12} = \frac{k_b}{m'_b\omega}\left(\frac{-\mathrm{j}2\sqrt{\tilde{\alpha}_b}}{1+\tilde{\alpha}_b}\right), \quad \tilde{\alpha}_b = \mathrm{e}^{-\mathrm{j}2\tilde{k}_b L_b} \tag{30a–c}$$

where k_b is the beam wavenumber. These mobilities are derived on the assumption that there are travelling waves in the beam together with a small near field. They are inappropriate if the beam carries complex waves and are also inaccurate at low frequencies due to the neglect at the drive point of the near field generated at the undriven end of the beam. Accordingly, these expressions are only considered accurate when the near field has decayed to 1% of its value at the undriven end, i.e., when $k_b L_b > 4.6$ or above 15 Hz for the structure of Figure 3.

The input and transfer mobilities of the finite spine beam attached to the finite receiver plate are

$$\tilde{Y}_{1\,psb} = \frac{k_{psb}}{(m'_b + m'_{px})\omega}\left(\frac{1-\tilde{\alpha}_{psb}}{1+\tilde{\alpha}_{psb}} - \mathrm{j}\right), \quad \tilde{Y}_{12\,psb} = \frac{k_{psb}}{(m'_b + m'_{px})\omega}\left(\frac{-\mathrm{j}2\sqrt{\tilde{\alpha}_{psb}}}{1+\tilde{\alpha}_{psb}}\right),$$

$$\tilde{\alpha}_{psb} = \mathrm{e}^{-\mathrm{j}2\tilde{k}_{psb}L_b} \tag{31a,b}$$

where k_{psb} is found from the dispersion relation of equation (25). In addition to the constraint on the value of the beam near field noted above, these expressions are only considered accurate above $k_p L_p > 9{\cdot}2$ (30 Hz for the structure in Figure 3) because of the neglect of the near field generated at the outer edges of the plate.

Equation (31) involves significant amounts of computation in which errors may arise. The input response can be checked approximately using the simpler characteristic mobility for a semi-infinite spine beam projecting away from the edge of a semi-infinite receiver plate

$$\tilde{Y}_1^{1/2\infty} = \frac{k_{psb}}{(m'_b + m'_{px})\omega}(1 - \mathrm{j}). \tag{32}$$

Equations (31) and (32) will be used in section 4 when the predicted frequency response functions of the plate-stiffened beam of Figure 3 are compared with laboratory measurements.

3. LABORATORY MEASUREMENTS ON TWO PLATE-STIFFENED BEAMS

Measurements of input and transfer accelerance had been made previously on a perspex plate-stiffened beam in reference [12] and some of these data are used in what follows. The plate was symmetric on either side of the beam merely for convenience. To augment the results from reference [12] and to determine the robustness of the theory in section 2, a second structure with slightly different parameters was also examined. The details of the two structures are as follows:

(a) *Structure* "*A*": This is the structure used in reference [12] with the dimensions of Figure 3 and a plate width $L_y = 1{\cdot}16$ m. The tolerance on the width was $\pm$ 3 mm. The structure was supported on a sheet of rubber foam to isolate it from the underlying laboratory bench. The foam also increased the plate loss factor to the value shown in Figure A2 (see Appendix A).

(b) *Structure* "*B*": This is the structure used in reference [12] but with the edges of the plate clamped very tightly between some very stiff steel channels [20] as shown in Figure 8. The perspex plate thickness varied by up to 10% from

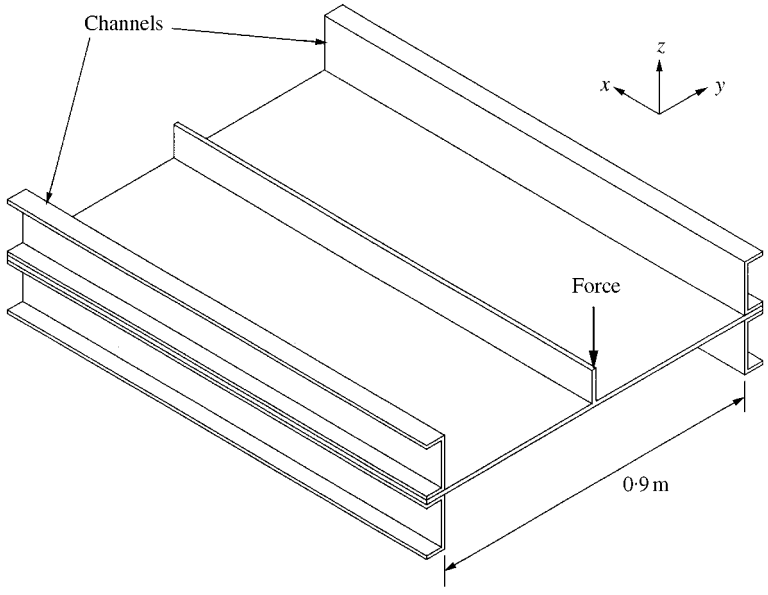

Figure 8. Sketch of the plate-stiffened beam structure "B" with the edges clamped between $76 \times 52 \times 10$ kg/m mild steel channels [20] using large G-cramps (not shown) on each side.

the nominal value shown in Figure 3 and the faces of the channels were not exactly flat either. Thus, the joints between the channels and the plate were filled with a thin layer of pipe jointing compound (e.g. reference [21]) to make them appear more fully clamped, especially at higher frequencies when the jointing compound would stiffen due to viscous action. The channels also reduced the width of the plate to $L_y = 0{\cdot}9$ m $\pm$ 2 mm. Because the structure was supported by the channels, the foam was removed from underneath the plate.

For comparison, Table 2 summarizes the configuration of the two structures. Figure 9 shows the finite receiver impedances calculated for the two structures from equation (23). Note that because the reflection coefficient is $\tilde{r} = -\mathrm{j}$ for both free and clamped edges [15] equation (23) is appropriate in both cases. The differing resonant and anti-resonant levels arise from the differing loss factors of the two plates. The different receiver widths account for the different frequencies of the anti-resonant peaks and resonant troughs.

Both plate-stiffened beams were excited at one end on the upper edge of the beam by a Brüel & Kjær type 8202 impulse hammer. To improve the quality of the impulse, a small steel wedge with a mass of 4 g was glued to the end of the beam. For the input accelerance, a small Brüel & Kjær type 4375 accelerometer (mass about 3 g) was fixed to the beam as close as possible to the wedge. For the transfer accelerance, an additional accelerometer was placed at the far end of the beam. The signals from the impulse hammer force gauge and the accelerometers were conditioned by Brüel & Kjær type 2635 charge amplifiers before being sent to

TABLE 2

The configuration of the two experimental plate-stiffened beam structures

Structure	Plate width L_y (m)	Boundary Condition of plate edge parallel with beam	Beam loss factor	Plate loss factor
A	1·16	Free	0·05	As in Figure A2 (see Appendix A)
B	0·9	Clamped	0·05	0·05

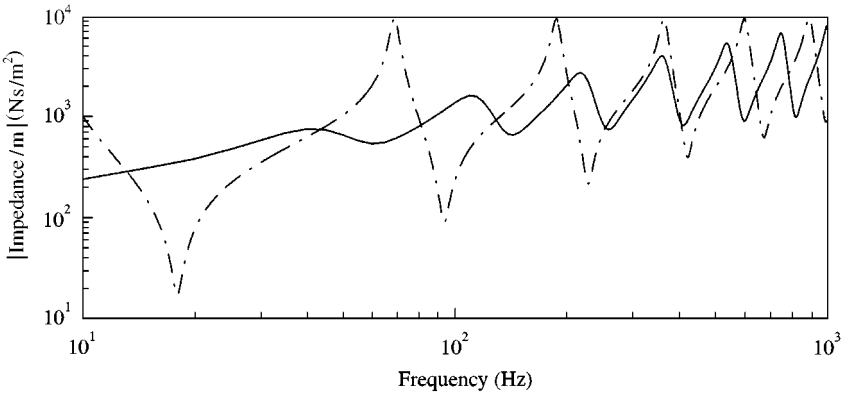

Figure 9. Input impedance per unit length of the receivers for the two plate-stiffened beams calculated using equation (23): ——, structure "A"; – · – · –, structure "B".

a digital spectrum analyser. For each measurement, 10 signals were acquired and the average response determined. The ordinary coherence function was checked to ensure that the data were of acceptable quality.

The frequency range of the measurements was 10 Hz to 1 kHz. The lower frequency limit was determined by the low accelerometer sensitivity. The upper frequency limit was governed by the constraint of Euler–Bernoulli beam theory used to derive the mobilities of equation (31). At 1 kHz, the flexural wavelength would be at least 10 times the depth of the beam so there was no risk of the motion tending toward that of a Timoshenko beam [15].

4. COMPARISON OF THE MEASURED AND PREDICTED RESPONSES

4.1. INPUT ACCELERANCE FOR STRUCTURE "A"

Figure 10 compares the predicted input accelerance for the structure in Figure 3 from equation (31a), the characteristic accelerance for the equivalent semi-infinite plate-stiffened beam using equation (32) and the measured response. The following observations are made.

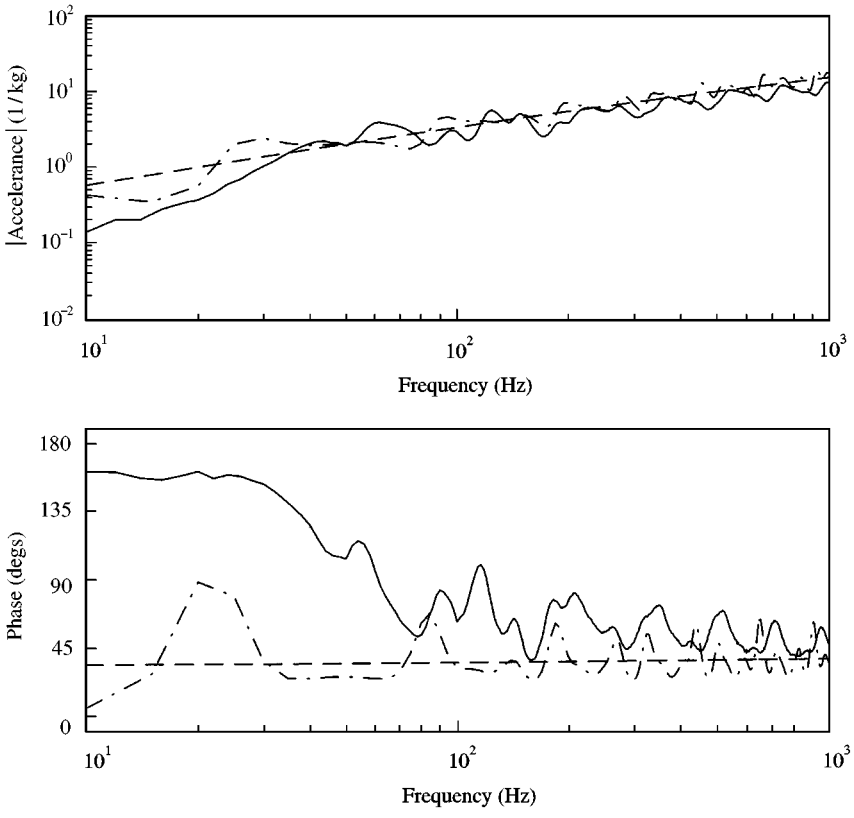

Figure 10. Input accelerance of structure "A" ——, measurement; – · – · –, prediction; – – –, characteristic accelerance using equation (32).

(a) Below 40 Hz, the measurement show a phase which is close to that of a pure stiffness caused by the entire structure moving on the rubber foam.

(b) The magnitude of the predicted characteristic accelerance of equation (32) follows the frequency average of the measurement up to 200 Hz but thereafter rises a little above the frequency average. This is believed to be due to the mass of the accelerometer and wedge located at the drive point [22].

(c) The peak and trough levels of the measurement and of the finite prediction are in good agreement once allowance for the discrepancy in the frequency-average level is accounted for. This indicates that the plate loss factor shown in Figure A2 is acceptable.

(d) Both the measured response and the finite prediction show a number of resonances but they are poorly defined due to the heavy damping. The measured phase shows some "peaks" such as at 105 and 210 Hz which are not visible in the prediction. In fact, the transfer accelerance discussed below will show that these peaks in the phase occur when the receiver is anti-resonant. At these frequencies, the input mobility in equation (31a) is not tenable because the travelling wave in the beam is heavily attenuated by the receivers and the near field is large.

4.2. TRANSFER ACCELERANCE FOR STRUCTURE "A"

Figure 11 compares the measured response with that predicted using equation (31b). The following observations are made:

(a) The prediction and measurement disagree below 40 Hz due to the stiffness of the rubber foam.
(b) Both measurement and prediction show narrow bands in which the response at the end of the beam is heavily attenuated. By comparing Figure 9 with Figure 11, it can be seen that the narrow bands of high attenuation coincide with the anti-resonances (i.e., the peaks) of the finite receiver impedance. This agreement supports the use of the estimated finite receiver wavenumber of equation (24) in equation (23).
(c) The predicted peak response lies above the measured peak response, especially at the higher frequencies, and the lowest amplitudes in the troughs are consistently under-predicted above 300 Hz. This discrepancy is likely to be caused by the limitations of equation (31b) when the receiver is anti-resonant, but it may also be due to the small variations in both the thickness and the width of the perspex plate which perturb its impedance

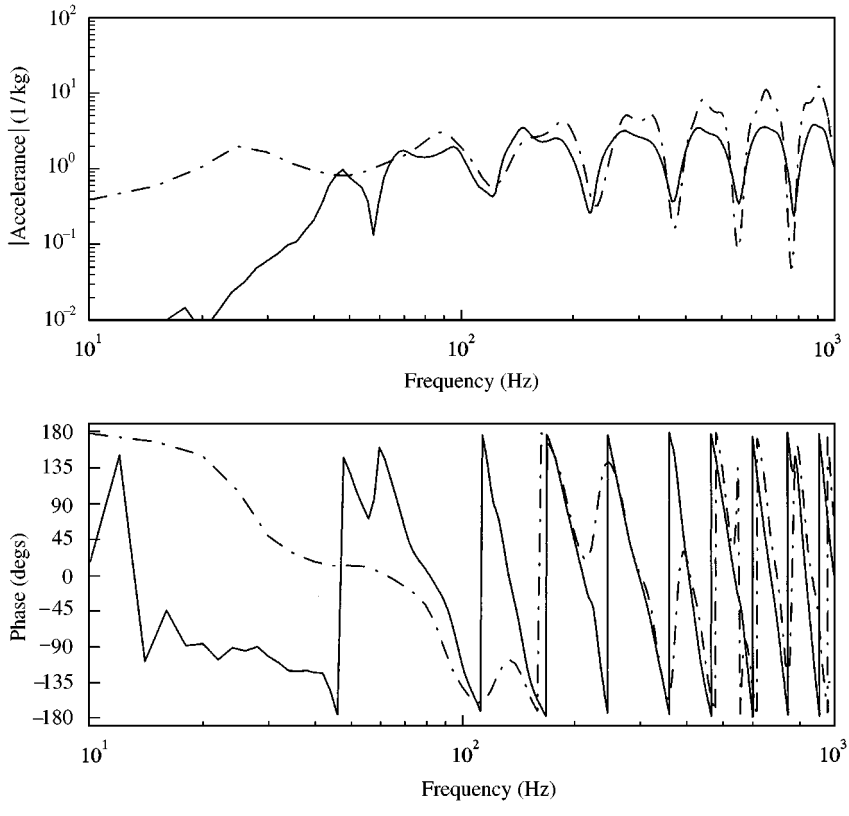

Figure 11. Transfer accelerance to the far end of structure "A" ——, measurement; – · – · –, prediction.

away from the receiver impedance of equation (23). These limitations also account for the inaccuracy of the predicted phase in the narrow bands.

(d) There is one narrow band in the measurement at 60 Hz which is not predicted. The receiver impedance in Figure 9 does exhibit a poorly defined anti-resonance around this frequency, but the plate damping may be overestimated in this region such that the magnitude of the receiver impedance is inaccurate.

Whilst the agreement between measured and predicted peak and trough levels is limited, the agreement of the frequencies of the narrow bands is very encouraging because it means that these narrow bands can be used in vibration control applications to limit the transmission of certain frequencies along the beam. In effect, the plate creates a set of narrow-band vibration neutralizers.

4.3. INPUT AND TRANSFER ACCELERANCES FOR STRUCTURE "B"

Figure 12 compares the measured and predicted input response of structure "B". The following observations additional to those for structure "A" can be made:

(i) In comparison with the two previous measurements, it is immediately apparent that the frequency-average damping of the beam is much lower.

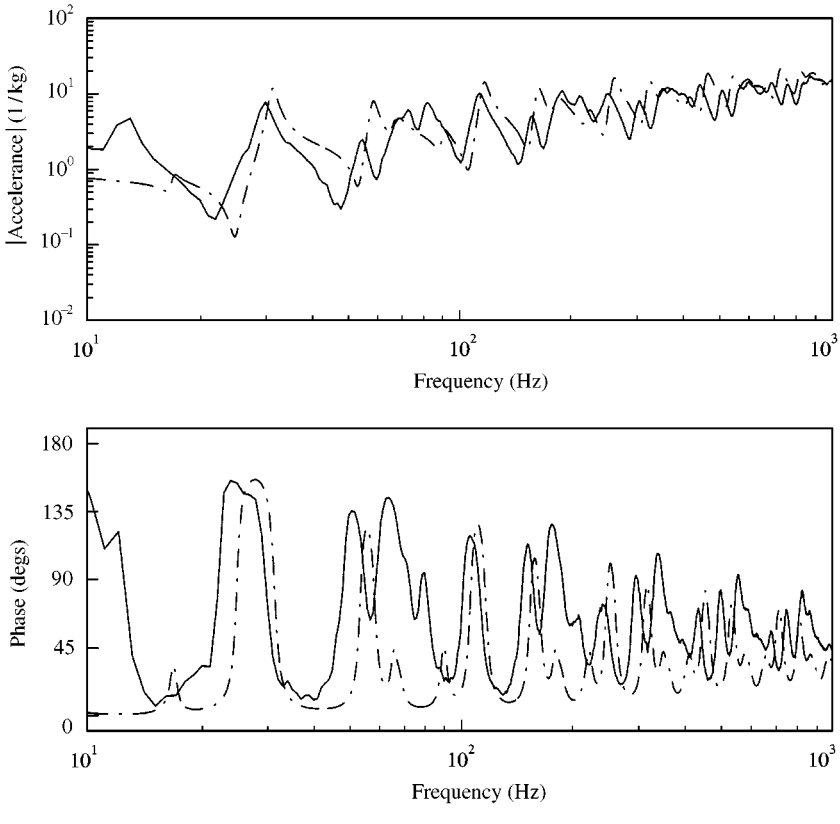

Figure 12. Input accelerance of structure "B": ——, measurement; – · – · –, prediction.

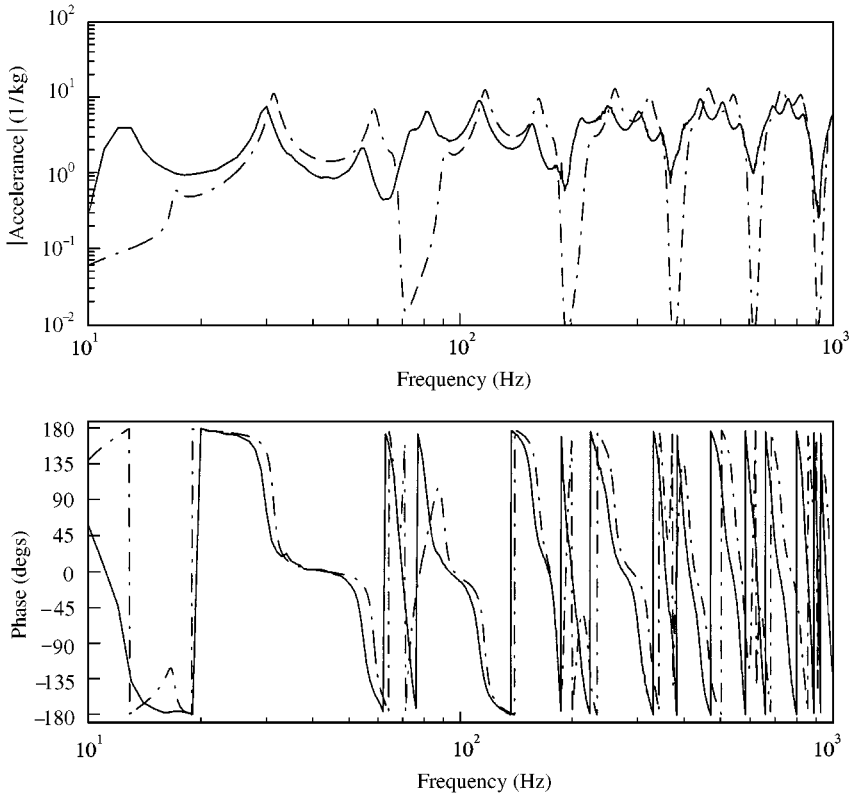

Figure 13. Transfer accelerance of structure "B": ——, measurement; – · – · –, prediction.

(ii) There is a 5% discrepancy between the predicted and measured frequencies of some of the large peaks such as at 110 Hz which suggests that the beam stiffness calculated using equation (16) is slightly inaccurate.
(iii) There are significant discrepancies in both magnitude and phase around 60–70, 200 and 400 Hz which coincide closely with the anti-resonances of the finite receiver impedance in Figure 9.

The transfer accelerance of Figure 13 shows features similar to those observed in the response of structure "A", illustrating once again that the plate creates a set of narrow-band vibration neutralizers. Collectively, these results support the theoretical method.

5. CONCLUDING REMARKS

A simple plate-stiffened beam consisting of a directly excited stiff spine beam attached to a large flexible receiver plate has been used to investigate the theory that a built-up structure carrying long-wavelength flexural waves in the directly driven spine and short wavelength flexural waves in the indirectly driven receiver can be analyzed by combining separate models of the spine and receiver. The results of this investigation are as follows.

(a) Provided the wavenumber in the receiver plate is at least twice the wavenumber in the spine beam, the receiver can be idealized as a set of independent plate strips which have a locally reacting receiver impedance given by equation (23).
(b) The receiver impedance is a function of two parameters: the length of the receiver normal to the spine and the receiver wavenumber which describes the radiation of waves into the receiver at an angle normal to the spine.

The method has been used to predict the input and transfer response of two slightly different plate-stiffened beams. These predictions have compared well with laboratory measurements. In particular, it has been demonstrated that when the beam is attached to a finite plate, the transmission along the beam is significantly reduced in narrow-frequency bands in which the plate is anti-resonant. In effect, the finite plate creates a set of narrow-band vibration neutralizers. The frequencies of these narrow bands of high attenuation have been predicted which means that they can be used in vibration-control applications.

REFERENCES

1. R. M. Grice and R. J. Pinnington 2000 *Journal of Sound and Vibration* **230**, 851–875. A method for the vibration analysis of built-up structures, Part II: Analysis of the plate-stiffened beam using a combination of finite element analysis and analytical impedances.
2. R. J. Pinnington 1988 *Technical Report No.* 162, *ISVR*, *Southampton University*. Approximate mobilities of built-up structues.
3. R. E. Powell and J. E. Manning 1988 59*th Shock & Vibration Symposium*, *Albuquerque*, *NM*, *U.S.A.* **1**, 89–102. The importance of in-plane and non-resonant energy transmission in statistical energy analysis.
4. F. J. Fahy and E. Lindqvist 1976 *Journal of Sound and Vibration* **45**, 115–138. Wave propagation in damped structures characteristic of ship construction.
5. B. M. Gibbs and P. G. Craven 1981 *Journal of Sound and Vibration* **77**, 429–435. Sound transmission and mode coupling at junctions of thin plates. Part II: parametric survey.
6. F. J. Fahy 1994 *Philosphical Transactions of the Royal Society of London A* **346**, 431–447. Statistical energy analysis: a critical overview.
7. B. M. Gibbs and C. L. S. Gilford 1976 *Journal of Sound and Vibration* **49**, 267–286. The use of power flow methods for the assessment of sound transmission in building structures.
8. R. H. Lyon 1985 *Noise Control Engineering Journal* **26**, 22–27. In-plane contribution to structural noise transmission.
9. G. L. Lamb 1961 *Journal of the Acoustical Society of America* **33**, 628–633. Input impedance of a beam coupled to a plate.
10. M. Heckl 1961 *Journal of the Acoustical Society of America* **33**, 640–651. Wave propagation on beam–plate systems.
11. H. Kuttruff 1979 *Room Acoustics*. Applied Science, second edition.
12. R. M. Grice 1993 *M.Sc. Thesis*, *University of Southampton*. Vibrational power transmission through ship hull and double bottom structures.
13. R. M. Grice and R. J. Pinnington 1995 *Proceedings Inter-Noise* 1995, *Newport Beach*, *Cal. USA*. Vibration power transmission in beam-stiffened plate systems.
14. Lord Rayleigh 1896 *The Theory of Sound*. New York: MacMillan.
15. L. Cremer, M. Heckl and E. E. Ungar 1988 *Structure-borne Sound*. Berlin. Springer Verlag. Second edition.

16. C. R. Fuller and F. J. Fahy 1982 *Journal of Sound and Vibration* **81**, 501–518. Characteristics of wave-propagation and energy-distributions in cylindrical elastic shells filled with fluid.
17. J. D. Achenbach 1973 *Wave Propagation in Elastic Solids*. Amsterdam: North-Holland.
18. R. J. Pinnington and R. G. White 1981. *Journal of Sound and Vibration* **75**, 179–197. Power flow through machine isolators to resonant and non-resonant beams.
19. V. Kolousek 1973 *Dynamics in Engineering Structures*. London: Butterworths.
20. British Standard 4: Part 1: 1993. *Structural Steel Sections*. London: British Standards Institute.
21. *Boss Green Pipe Joining Compound*. Leicester, England: BSS (UK) Ltd.
22. R. M. Grice 1998 *Ph.D. Thesis, Southampton University*. Vibration analysis of built-up structures by combining finite element analysis and analytical impedances.
23. R. J. Pinnington 1982. *Ph.D. Thesis, Southampton University*. Vibrational power transmission between sources and substructures.
24. L. C. Chow and R. J. Pinnington 1987 *Journal of Sound and Vibration* **118**, 123–139. Practical industrial method of increasing structural damping in machinery, I: squeeze film damping with air.

APPENDIX A: MEASUREMENT OF THE LOSS FACTOR FOR PERSPEX WHEN VIBRATING IN AIR AND WHEN LYING ON RUBBER FOAM

This appendix describes the procedure used to determine the loss factor of the perspex plate of the plate-stiffened beam for the measurements presented in section 4.

For a moderately or heavily damped structure, traditional methods for calculating the loss factor such as the Argand diagram or the half power-point bandwidth method [15] are unreliable. In such cases, a more accurate determination of the damping is obtained using the difference between the maximum and minimum levels of the real part of the input mobility [23].

The input an Euler–Bernoulli beam is [18, 19]

$$\tilde{Y}_1 = \frac{k_b}{m'_b\omega}\left(\frac{1-\tilde{\alpha}}{1+\tilde{\alpha}} - \mathrm{j}\right), \quad \tilde{\alpha} = \mathrm{e}^{-\mathrm{j}2\tilde{k}_b L_b}, \quad k_b L_b > 4{\cdot}6. \tag{A1}$$

The real part of the input mobility cycles between maximum values

$$\mathrm{Re}\{\tilde{Y}_1\} = \frac{k_b}{m'_b\omega}\left(\frac{1+\alpha}{1-\alpha}\right), \quad \alpha^{-\eta_b k_b L_b/2} \tag{A2}$$

and minimum values

$$\mathrm{Re}\{\tilde{Y}_1\} = \frac{k_b}{m'_b\omega}\left(\frac{1-\alpha}{1+\alpha}\right). \tag{A3}$$

The ratio of the maximum to minimum values at any frequency is therefore

$$Q = \left(\frac{1+\alpha}{1-\alpha}\right)^2. \tag{A4}$$

Thus, the loss factor of the beam η_b is

$$\eta_b = -\frac{2}{k_b L_b}\ln\left(\frac{\sqrt{Q}-1}{\sqrt{Q}+1}\right). \tag{A5}$$

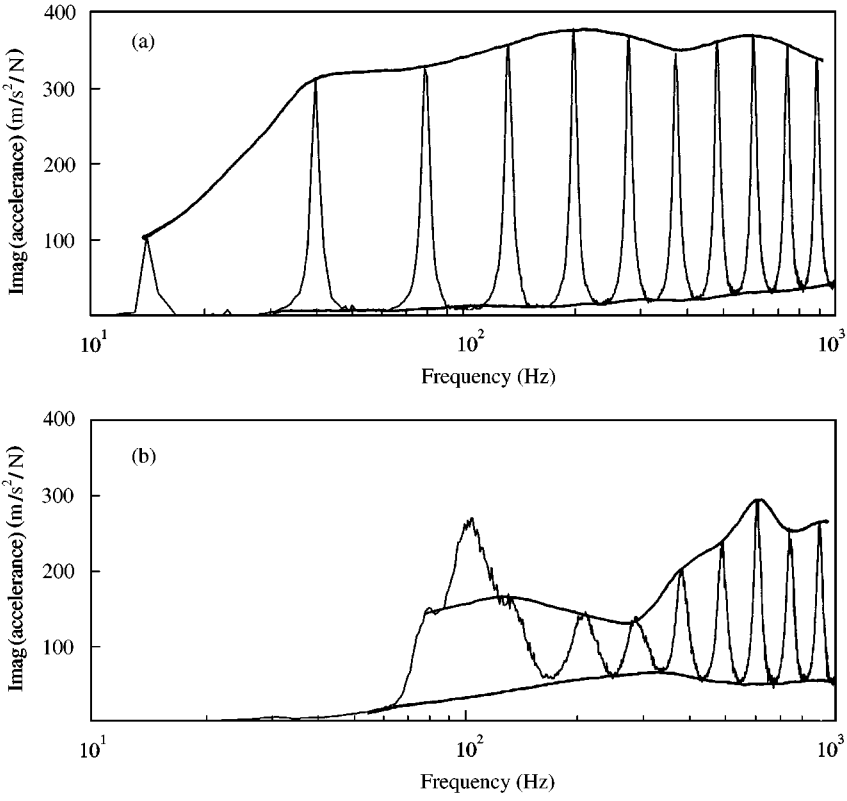

Figure A1. Imaginary parts of the input accelerance and envelopes of maxima and minima for the perspex beam vibrating in air or lying on rubber foam: (a) beam vibrating in air; (b) beam lying on rubber foam.

To apply this technique, two smooth envelopes are drawn on a graph of the real part of the measured input mobility, one through the maxima and the other through the minima. At any frequency, the maximum to minimum ratio is found and equation (A5) utilized to calculate the loss factor.

To measure the loss factor for the perspex of the plate-stiffened beam, a uniform beam with dimensions $0{\cdot}9\ \text{m} \times 0.027\ \text{m} \times 0.0059\ \text{m}$ was made using a piece of perspex from the structure. Two measurements were made: the first with the beam suspended in air in order to measure the nominal material loss factor, the second with the beam lying on a sheet of rubber foam identical to that used to support the plate-stiffened beam in section 3. In both cases, a miniature Brüel and Kjær Type 4374 accelerometer was attached using beeswax to one end of the beam. At the same end of the beam but on the opposite side to the accelerometer, the beam was excited using a Brüel and Kjær Type 8202 impact hammer. The input accelerance was measured using a spectrum analyser.

Figure A1(a) shows the real part of the input accelerance of the beam vibrating in air together with the maximum and minimum envelopes. Figure A2 shows the loss factor calculated using equation (A5) at four frequencies. The loss factor appears to fall by 20% with frequency, but for the purposes of the predictions in section 4 it was assumed constant at 0·05.

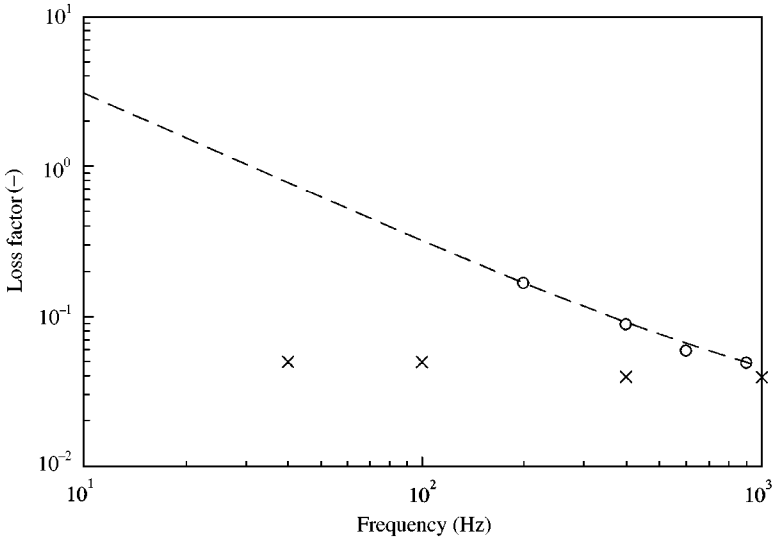

Figure A2. Measured loss factors for the perspex beam: ×, beam suspended in air; ○, beam lying on rubber foam; – – –, curve fitted to the rubber foam loss factor data.

Figure A1(b) shows the real part of the input accelerance of the beam vibrating on the foam. It can be seen that below 60 Hz there is no clear maximum and minimum envelope. Therefore, the beam is virtually semi-infinite in this frequency range. The resonance at 100 Hz does not follow the frequency spacing of the other resonances and is probably a torsional mode. Hence, the envelope of the maxima was drawn through the peaks of the two resonances at 80 and 120 Hz. Between 200 and 400 Hz the damping is clearly very high before falling with frequency. Figure A2 shows the loss factor calculated at four frequencies together with a best-fit curve. The values above 200 Hz vary approximately inversely with frequency. This result is consistent with theoretical and measured results for a plate lying on air-filled ceramic fibre insulation which is dynamically similar to the open cell rubber foam used to provide the damping in the present case [24].

APPENDIX B: NOMENCLATURE

A tilde " $\sim$ " over a symbol indicates that it is, in general, complex.

A	wave amplitude (m)
b	width (m)
B	wave amplitude (m)
C	wave amplitude (m)
D	beam stiffness (N m); plate stiffness (N m^2)
E	Young's modulus of elasticity (N/m^2)
f	circular frequency (Hz)
f'	Force per unit length (N/m)
h	height (m)

j	$\sqrt{-1}$
k	wavenumber (m^{-1})
L	length (m)
m'_b	mass per unit length (kg/m)
m''_p	mass per unit area of a plate (kg/m^2)
Q	ratio of peak mobility to trough mobility (−)
$\tilde{r}$	reflection coefficient (−)
t	time (s); thickness (m)
u	displacement (m)
x, y, z	co-ordinates
Y	structural mobility (m/sN)
Z'	structural impedance per unit length (N s/m)
$\tilde{\alpha}, \tilde{\beta}$	travelling wave attenuation coefficients (−)
η	structural loss factor (−)
η_{12}	coupling loss factor (−)
λ	wavelength (m)
ν	Poisson's ratio (−)
ρ	density (kg/m^3)
ω	radian frequency (rad/s)